Experimental investigation of magma rheology at 300 MPa: From pure hydrous melt to 75 vol. % of crystals.

Rémi Champallier, Misha Bystricky, Laurent Arbaret

Experimental investigation of magma rheology at 300 MPa: From pure hydrous melt to 76 vol. % of crystals.

Rémi CHAMPALLIER [a, *] , Misha BYSTRICKY [b, c] , Laurent ARBARET [a]

[a] Institut des Sciences de la Terre d'Orléans, UMR 6113 CNRS/INSU, Université d'Orléans, 1a rue de la Férollerie, 45071 Orléans Cedex 02, France

[b] LMTG, Université de Toulouse, CNRS, IRD, Observatoire Midi-Pyrénées, 14 Av. E. Belin, F-31400 Toulouse, France

[c] Geologisches Institut, Sonneggstrasse 5, ETH Zürich, CH-8092 Zürich, Switzerland

* Corresponding author: Tel: +33-2-38-25-53-44; Fax: +33-2-38-63-64-88

E.mail addresses: champa@cnrs-orleans.fr , bystricky@lmtg.obs-mip.fr , laurent.arbaret@univ-orleans.fr

Abstract

The rheological behaviour of synthetic crystal-bearing magmas containing up to 76 vol.% of crystals ($0 \leq \phi_S \leq 0.76$) has been investigated experimentally at a confining pressure of 300 MPa and temperatures between 475 and 1000°C at shear rates between 10^{-4} and $2x10^{-3}$ s^{-1}. Starting hydrated crystal-bearing glasses were synthesized from a dry haplogranitic glass ($Qz_{36}Ab_{39}Or_{29}$) and 2.5 wt.% water mixed with 0 (pure hydrous melt), 16, 34, 54, 65 or 76 vol.% of Al_2O_3 sieved ($45 < Ø < 90$ μm) crystals. Shear viscosity measurements were performed in torsion (simple shear) in a Paterson gas-medium apparatus.

For pure hydrated melt and for 16 vol.% of crystals, the rheology is found to be newtonian. At higher crystal contents, the magmas exhibit shear thinning behaviour (pseudoplastic). The Einstein-Roscoe equation adequately estimates viscosities of the crystal-bearing magmas at low crystal contents ($\phi_S \leq\sim 0.25$), but progressively deviates from the measured viscosities with increasing crystal content as the rheological behaviour becomes non-newtonian. On the basis of a power-law formulation, we propose the following expression to calculate the viscosity as a function of temperature, crystal content and applied stress (or shear rate):

$$\dot{\gamma} = A_0 (1 - \Phi / \Phi_m)^K \, \tau^{(1+K_1 \Phi^{K_2})} \exp\left(\frac{-Q}{RT}\right),$$

where $\dot{\gamma}$ is shear rate (s^{-1}), τ is shear stress (MPa), Φ is the crystal volume fraction, T is temperature (K), Φ_m is the relative maximum packing density, R is the gas constant, Q = 231 $kJ.mol^{-1}$ is the activation energy of the viscous flow and A_0, K, K_1 and K_2 are empirical parameters.

Keywords: rheology, viscosity, magma, crystals fraction, experimental petrology, non-Newtonian.

1. Introduction

Viscosity of magmas is recognized as a critical factor controlling magma ascent and emplacement in the Earth's crust and eruptive styles of volcanoes. An important goal during the last 40 years has been to measure and model the viscosity of silicate liquids [1-15]. However, although most natural magmas are crystal suspensions, studies on the effect of crystals on the rheological properties of magmas have long been scarce [16-19] until the late nineties [20-29]. Despite these new data, the existence, significance and importance of some rheological thresholds are still under debate [30-32] and a unified model for predicting the viscosity of magmas over their whole range of crystallisation is still to be proposed.

At low crystal contents, it is generally assumed that magmas can be approximated as Newtonian fluids (e.g. [33]) and that their viscosity can be estimated according to the Einstein-Roscoe equation [34-37]:

$$\eta = \eta_0 (1 - \Phi_s/\Phi_m)^{-k} \quad , \qquad \text{(E1)}$$

where η_0 is the viscosity of the melt, Φ_s the crystal fraction, Φ_m the maximum packing fraction of crystals and k an adjustable parameter. However, the value of Φ_m depends on the size, shape and distribution of crystals [21, 38, 39] and has been extensively debated in the literature. For suspensions of particles in a fluid, values of Φ_m in the range 0.32 to 0.71 have been measured [40], while values between 0.5 and 0.7 are considered realistic for magmas [41]. Moreover, [21] highlight that Φ_m and k are interdependent when adjusting (E1) to experimental data.

At higher crystal contents, the rheological behaviour of magmas is no longer Newtonian and two phenomena are classically described and discussed. First, many studies report that the development of a 3-D framework of crystals inhibits flow movement at low stresses, causing a yield strength to appear (e.g. [22, 40]). Studies based on the percolation theory show that the

value of the critical (crystal) volume fraction Φ_c for the onset of crystal or particle networks, which depends on particle shape and size distributions and on the particles' overall orientation distribution [42-45], can be as low as $\Phi_c = 0.08$ for highly anisotropic particles [45, 46]. Second, apparent viscosities depend on shear rate for high-concentration suspensions [21, 27, 28, 39, 47] and the nature of this dependence is still not well understood.

In the present study, we investigate the rheological behaviour of synthetic magmatic suspensions containing up to 76 vol.% of crystals. Viscosity measurements are conducted under a confining pressure (300 MPa) in simple shear (torsion) in a servo-controlled internally-heated high-pressure deformation vessel (Paterson apparatus). The effect of temperature (475°C ≤ T ≤ 600°C) and of shear rate (10^{-4} s^{-1} ≤ $\dot{\gamma}$ ≤ 2x10^{-3} s^{-1}) on viscosity are characterized as a function of crystal content. Our data are compared with previous studies and are used to test the model proposed by [40] for the viscosity of crystal-bearing magmas. The evolution of viscosity with increasing crystal content is discussed. Moreover, the development of microstructures studied in a companion paper [48] is presented and correlated with the rheological behaviour.

2. Experimental Methods

2.1. Starting material and analytical techniques

Starting crystal-bearing hydrated glasses with a crystal fraction of up to 76 vol.% ($0 \leq \phi_S \leq 0.76$) were prepared following the procedure of [49]. A finely ground powder of dry haplogranitic glass (SiO_2: 78.8, Al_2O_3: 12.4, Na_2O: 4.6, K_2O: 4.2 wt.%, microprobe analyses) prepared by Schott AG (Germany) was mixed with 0, 16, 34, 54, 65 or 76 vol.% of Al_2O_3 sieved ($45 < \phi < 90$ μm) crystals (insulating powder from Friatec AG, Germany - Corundum). The glass + crystal mixture was loaded in large gold capsules (20 mm in diameter and 35 mm in length) with demineralised water. The amount of added water was calculated to obtain 2.5

wt. % in melt in the final product independently of solid fraction. Capsules were arc-welded while surrounded by liquid nitrogen in order to prevent water loss. Melt hydrations were performed at IST Orléans in a large bore furnace of an internally heated pressure vessel (IHPV) at 1000°C and 100 MPa during 1 month, then isobarically quenched.

Observation of polished sections of the starting products shows that insignificant chemical reaction occurred between the melt and the crystals during hydration due to the subaluminous composition of the melt (molar $Al_2O_3/(Na_2O+K_2O)=1.025$) [49]. As expected due to the limited solubility of aluminium in subaluminous melts [50], microprobe analyses show a small enrichment in Al_2O_3 of the melt (less than 1.5 wt.%) in samples containing corundum crystals compared to the crystal-free hydrous melt. After hydration, all samples contain some residual bubbles (Figure 1). For the crystal-free starting product (HPG-10), the volume fraction of bubbles (Φ_b) was determined by image analysis of polished sections (Figure 1a) to be less than 0.01. For crystal-bearing starting products, determination of ϕ_b is not very accurate because the polishing procedure causes plucking of alumina grains, and it is often impossible to distinguish plucked grains from bubbles (Figure 1c).

The H_2O content of the starting products was controlled by Karl-Fisher titration (KFT) and by Fourier-transform infrared (FTIR) on some samples (see Table 1). The precision of KFT analyses is known to be ± 0.15 wt% H_2O and depends mainly on the amount of sample available and on measurement duration [51]. For crystal-bearing samples, it also requires a correction for crystal content.

FTIR analyses were performed on doubly polished glass plates using a Nicolet 760 Magna FTIR spectrometer. Spectra were collected with 128 scans, with a resolution of 4 cm^{-1}, a gain of 4, a CaF_2 beamsplitter, visible light, and a liquid N_2 cooled MCT/A detector. The concentrations of OH and H_2O species were determined by the peak heights of the absorption

bands at 4500 and 5200 cm^{-1}, respectively, using molar absorptivities from [52] for haplogranitic compositions. Glass densities were determined using the model of [53].

2.2. Viscosity measurements

Shear viscosity measurements were performed in torsion in an internally-heated gas medium deformation apparatus (Paterson instrument, Australian Scientific Instrument) at ETH Zurich. For these experiments, cylinders (8 to 15 mm in diameter) were cored in the synthesised starting products, then cut in 2 or 3 parts (5 to 12 mm in length). Opposite faces of the cylinders were finely polished in order to achieve parallelism within ± 3 μm, then inserted in a column assembly made of alumina and zirconia pistons enclosed in a copper or iron jacket. A 25 μm platinum foil was inserted between the specimen and the jacket in order to avoid chemical interactions at the high temperatures achieved during the experiments. The column assembly was placed in the Paterson apparatus so as to locate the sample in the large isothermal zone (±1°C over 5 cm) of the apparatus. Argon was used as the confining medium. Torsion was applied by an external motor controlled by a servo-motor and transmitted to the sample by the piston assembly. The torque applied to the sample was monitored without distortion by an internal load cell with a resolution of 0.1 N.m (see [54] for details).

As the sample was deformed together with the jacket (Figure 1d), a correction corresponding to the torque required to deform the jacket had to be applied to the recorded torque. The corrections were calculated using the deformation laws for copper and iron [55] modified after laboratory calibrations.

In this study, most experiments were multi-step measurements (Figure 2). At a given temperature, the torque M (N.m) was measured at different constant twist rates $\dot{\theta}$ ($rad.s^{-1}$); then the temperature was changed. On several occasions, the same conditions of temperature and twist rate were investigated a second time in order to test reproducibility.

3. Results.

3.1. Principle of data analysis.

Six sets of experiments were performed on samples containing 0, 16, 34, 54, 65 and 76 vol.% crystals embedded in a hydrous haplogranitic melt (2.5 wt.% H_2O in melt). For each type of sample, rheological data can be described by a flow law of the form [56]:

$$\dot{\gamma} = A\tau^n \exp(-Q/RT), \qquad \text{(E2)}$$

where $\dot{\gamma}$ is shear rate (s^{-1}), τ is shear stress (MPa), T is temperature (K), R is the gas constant (R = 8.31 $J.K^{-1}.mol^{-1}$), and A, n and Q are empirical parameters defined as the preexponential term, the stress exponent and the activation energy ($J.mol^{-1}$), respectively.

$\dot{\gamma}$, τ, and parameters n, Q and A are calculated from twist rate vs. torque data as follows [54]:

$$\dot{\gamma} = \frac{r\dot{\theta}}{l}, \qquad \text{(E3)}$$

where $\dot{\theta}$ is the angular displacement rate or twist rate (rad s^{-1}), r is the radius of the specimen (m) and l is its length (m).

The stress exponent n corresponds to the slope of a Log-Log plot of $\dot{\theta}$ vs. M at constant temperature (Figure 3):

$$n = \frac{d\ Log\ \dot{\theta}}{d\ Log\ M}, \qquad \text{(E4)}$$

To compare $\dot{\theta}$ vs. M data from different experiments, $\dot{\theta}$ and M have to be normalised to standard length and radius using the following equations:

$$\dot{\theta}_N = \dot{\theta}_m \frac{r_m}{l_m}\frac{l_N}{r_N}, \qquad \text{(E5)}$$

$$M_N = M_m \left(\frac{r_N}{r_m}\right)^3, \qquad \text{(E6)}$$

where r_m and l_m are the measured radius and length of the sample, $\dot{\theta}_m$ and M_m are the measured twist rate and torque, r_N and l_N are the standard radius and length and $\dot{\theta}_N$ and M_N are the normalised twist rate and torque, respectively.

Knowing the stress exponent *n*, the stress τ (Pa) can be calculated from the torque *M* from:

$$\tau = M \frac{(3 + 1/n)}{2\pi r^3}, \qquad \text{(E7)}$$

where *r* is the radius of the sample (m). Thus, once *n* is determined, typical stress vs. strain curves can be drawn (Figure 4), and the apparent viscosity η_a (Pa.s) at a given shear rate is given by:

$$\eta_a = \frac{\tau}{\dot{\gamma}}, \qquad \text{(E8)}$$

Q can be determined at constant stress using the expression:

$$Q = -R \ln(10) \frac{d\, Log\, \dot{\gamma}}{d\,(1/T)} \qquad \text{(E9)}$$

Having determined *n* and *Q*, *A* can be deduced from (E2).

For each step of each experiment, $\dot{\theta}$, *M*, $\dot{\gamma}$, τ, η_a and the step strain γ are summarised in Table 2. For each composition, the calculated *A*, *Q* and *n* values are presented in Table 3. The data are presented in the following sections.

3.2. Pure hydrous melt ($\phi_S = 0$).

For pure hydrous melt ($\phi_S = 0$), a single experiment (PO540) was conducted at 475°C and 500°C at shear rates ranging from 2×10^{-4} to 10^{-3} s^{-1} (Table 1). Figure 2 shows that at constant temperatures the torque increases when increasing shear rate and that, for equivalent shear rates, the torque becomes higher when decreasing temperature. Duplicate steps (steps 1 and 4 at 500°C and 5 and 8 at 475°C) show good reproducibility of measurements within the same

experiment. The discrepancies between steps 1 and 4 and steps 5 and 8 results in differences of only 0.07 and 0.04 Log Pa.s, respectively.

Data reported on a Log-Log plot of normalized twist rate $\dot{\theta}_N$ vs. normalized torque M_N in Figure 3a show a slope of n = 1.08 and 0.90 at 475°C and 500°C, respectively. This suggests that, within experimental errors, the rheology of the pure hydrous melt is approximately Newtonian (n =1) at both temperatures in the investigated range. As suggested by the form of the flow law (E2), the stress exponent n seems to be independent of temperature.

Assuming a stress exponent of 1, viscosities between $10^{10.83}$ and $10^{10.93}$ Pa.s were inferred at 475°C (Table 2). At 500°C, viscosity is about half a Log unit lower, bracketed between $10^{10.28}$ and $10^{10.35}$ Pa.s.

Figure 4a and 4b shows that for each measurement, the shear strain (γ) was large enough to allow stresses to reach an apparent steady-state value. At 475°C, reproducibility of measurements is clearly established for the two steps at 6.2 x 10^{-4} s^{-1} (Figure 4a). At 500°C, the second step at 6.2 x 10^{-4} s^{-1} is 2.9 MPa lower than the first one, however, resulting in a deviation of only 0.03 Log Pa.s.

Following the analysis procedure described in section 2.1, we obtain an activation energy (Figure 5) and a preexponential term of 252 kJ.mol^{-1} and $10^{12.7}$ MPa^{-1}s^{-1}, respectively, leading to the following flow law for pure hydrous haplogranitic melt:

$$\dot{\gamma} = 10^{12.7\pm1.3}\ \tau^{1.0\pm0.1}\ \exp\left(\frac{-252\pm19\ \text{kJ.mol}^{-1}}{RT}\right), \qquad \text{(E10)}$$

For all calculations described above, experiment step-number 3 (500°C, 2.1 x 10^{-4} s^{-1}) was not considered because contribution of the jacket (2.4 N.m) represents more than half of the global torque (4.6 N.m) recorded during this step (see Table 2). Experimental uncertainty was considered to be too high in this case.

3.3. Crystal-bearing melts.

3.3.1. Comments on experiments.

For the composition containing 16 vol. % of crystals (ϕ_S=0.16), 3 different experiments (PO514, PO519 and PO610) were conducted using two different starting samples (see Table 1). Two pieces were cored in sample HPG5 for experiments PO514 and PO519, while sample HPG11 was used for run PO610. As HPG5 and HPG11 do not have the same water content (2.6 and 3 wt% H_2O, respectively), data from the 3 experiments are not strictly comparable. In addition, for step 1 of PO519 and steps 3, 5, 6 and 7 of PO610, the contribution of the jacket is too high and these steps were not considered for calculations. In experiment PO609 on a sample containing 34 vol. % of crystals (Φ_s = 0.34), one data point was also discarded (step 4, 550°C and 2 x 10^{-4} s^{-1}) for the same reason. For Φ_s = 0.54, 3 experiments (PO516, PO524 and PO528) were performed on samples of different diameters in order to optimise the measurement range. Experiment PO612 was conducted with a sample containing 65 vol. % of crystals. At the beginning and the end (steps 1, 2, 9, 10, 11 and 12) of this experiment, a technical problem occurred, consisting of slipping at the interface between two alumina pistons. Thus the twist rate measured during these steps did not fully reflect deformation of the sample. This lead to an overestimation of the deformation of the sample and prevented determination of sample viscosity during these steps. Two runs were conducted at several temperatures and twist rates to deform a sample with 76 vol. % of crystals (PO515), but slip at piston interfaces occurred systematically under all applied conditions so that it was impossible to measure the strength of this sample. A total strain of approximately 0.05 was determined for this sample after the experiments by measuring the offset of strain markers on the jacket.

3.3.2. Stress exponent *n*.

For the composition containing 16 vol. % of crystals, data from experiment PO519 are not used because of the difference in water content between the starting products used in PO519 and PO610 (see above). Only 2 measurements were done at 475°C resulting in poor precision of the determination of the stress exponent. However data at 475°C and 500°C are in good agreement with a stress exponent of 1.13 in both cases (dotted lines in Figure 3b). For Φ_s = 0.34, stress exponents of 1.27 and 1.22 are determined at 500 and 550°C, respectively. At crystal fractions larger than 0.34, we observe highly non-Newtonian flow behaviour, with stress exponents of n = 2.02 (T = 550°C) and 2.18 (T = 600°C) for Φ_s = 0.54 and n = 2.98 (T = 600°C) for Φs = 0.65 (Figure 3).

3.3.3. Apparent viscosities η_a.

At Φ_s = 0.16 and 475°C, measured apparent viscosities are close to the ones recorded for pure hydrous melt ($10^{10.80}$ and $10^{10.94}$ Pa.s at 6.3 x 10^{-4} and 2.0 x 10^{-4} s^{-1}, respectively). At 500°C, the apparent viscosity measured in experiment PO519 is 0.2 Log unit higher than for pure hydrous melt under the same experimental conditions, while apparent viscosities measured in PO610 are lower. We attribute this discrepancy to the higher water content of the sample HPG11a that was used in PO610 (see Table 1). Comparison of experiments PO519 and PO609 shows that increasing crystal content from 16 to 34 vol.% increases the apparent viscosity by 0.3 Log units (e.g. steps at 6x10^{-4} s^{-1} at 500°C and 550°C). Due to the strongly non-Newtonian behaviour of crystal-bearing magmas at high crystal content, variations in apparent viscosities between Φ_s = 0.34 and Φ_s = 0.54 become sensitive to shear rate. The variation becomes weaker when shear rate increases. For example, at 550°C the difference is equal to 0.9 Log units at 2 x 10^{-4} s^{-1}, and drops to 0.7 Log units at 6.3 x 10^{-4} s^{-1} and to 0.5 Log

units at 2 x 10^{-3} s^{-1}. The same phenomenon is observed between $\Phi_s = 0.54$ and $\Phi_s = 0.65$, with an increase in apparent viscosities of about 0.5 up to 0.8 Log unit depending on shear rate.

3.3.4. Activation energy *Q* and preexponential factor *A*.

The activation energy *Q* remains nearly constant between 208 and 252 kJ.mol^{-1} over the whole range of investigation (Figures 5 and 6a) and no clear dependence on crystal content Φ_s could be demonstrated. The preexponential term *A* decreases when crystal fraction increases (Table 3).

3.3.5. Global Fitting.

The least-square regressions described in the previous sections give a flow law for each crystal fraction investigated. On the basis of these flow laws, we propose a modification of (E2) that provides:

$$\dot{\gamma} = A_\Phi \, \tau^{n_{\Phi_s}} \exp\left(\frac{-Q}{RT}\right), \qquad \text{(E11)}$$

which includes the crystal content Φ_s as a variable. Since the activation energy remains nearly constant over the whole range investigated (Figure 6a), it is fixed at its weighted mean value (231 ± 19 kJ.mol^{-1}). Then, the stress exponent n_{Φ_s} is fitted (Figure 6b) to an expression of the form:

$$n_{\Phi_s} = 1 + K_1 \Phi_s^{\,K_2}, \qquad \text{(E12)}$$

where n_{Φ_s} the stress exponent at a given concentration of solid phase (Φ_s), and K_1 and K_2 are empirical parameters equal to 9.95 ± 2.63 and 4.50 ± 0.54, respectively. The preexponential

term (Figure 6c) is fitted to an expression approaching the form of the Einstein-Roscoe equation [34-37]:

$$A_\Phi = A_0(1-\Phi_s/\Phi_m)^K, \qquad \text{(E13)}$$

where A_Φ is the preexponential term at Φ_s and Φ_m is the maximum particle packing concentration. The fit to (E13) yields the values Log A_0 = 11.52 ± 0.2, Φ_m = 0.66 ± 0.01 and K = 4.0 ± 0.7.

These equations are valid only for haplogranitic crystal-bearing melt containing 2.5 wt. % of water. However, we argue that changes in the melt composition or water content will mainly affect the activation energy term Q and the value of A_0, the terms reflecting the viscosity of the pure melt.

4. Discussion.

4.1. Comparison with previous studies.

Figure 7 shows measured apparent viscosity (filled diamonds) versus crystal concentration at 500°C and a shear rate of 6 x 10^{-4} s^{-1}. On this figure are also reported the viscosity of a pure (Φ_s = 0) haplogranitic melt with 2.3 wt.% of water at 502°C [6] and viscosities of partially crystallised $Mg_3Al_2Si_3O_{12}$ melts ($\Phi s \leq 40\%$) at 800°C [21]. This data set was chosen because the viscosity of pure $Mg_3Al_2Si_3O_{12}$ melt (Φs = 0) at 800°C is similar to the viscosity of our hydrous haplogranitic melt at 500°C, allowing us to compare directly the effect of solid fraction on viscosity in the two series of crystal-bearing magmas. The Einstein-Roscoe model is given for comparison (dashed line).

For pure hydrous melt, our measurement is in very good agreement with data from [6], considering the small differences in temperature and in water content in both samples. This agreement validates the use of the Paterson apparatus, which was initially designed for

deformation experiments on solid aggregates, for viscosity measurements on supercooled liquids.

For crystal-bearing magmas with a low crystal content (i.e. up to Φs = 0.25 – 0.3), our data are in good agreement with data of [21]. At higher crystal content, a significant deviation is observed, viscosities measured in our study being lower than the ones obtained by [21]. This deviation may be attributed to several factors which are different between the two studies. First, the deformation geometry is not the same. Samples were deformed in compression (coaxial deformation) in [21] and in torsion (simple shear) in the present study. This factor may influence the development of shape preferred orientations of crystals (SPO), potentially resulting in differences in measured bulk viscosities. Second, shape, size and roughness of particles are different in the two studies, and morphological characteristics of particles have been shown to influence the viscosity of crystal-bearing magmas [33, 40, 57, 58]. Deformation rate is another difference between the two studies, and it is well established that, for high-concentration suspensions, viscosities at low and high strain rates can differ considerably for high-concentration suspensions [39, 40, 47].

Overall, our results are in good agreement with previous experimental studies and numerical simulations. At low crystal concentrations (Φ_s < 25 vol.%), crystal-bearing magmas can be approximated as Newtonian fluids [19, 21, 59, 60] and viscosities increase with increasing crystal content according to the Einstein-Roscoe equation (E1).

At higher crystal contents, the observed rheology is clearly no longer Newtonian and our crystal-bearing suspensions can be viewed as pseudoplastic materials whose behaviour is described by a power law with a stress exponent n >1 (Figure 8). However, it is widely assumed that a yield strength appears once a 3D-framework of crystals develops and our suspensions at high crystal fractions may be viscoplastic materials (pseudoplastic with a yield stress). Unfortunately it was impossible in our study to determine yield strength because

experiments were run at high stresses. Data at lower stresses are required to precisely determine if a yield power-law is more appropriate.

Time-dependent behaviour (thixotropy) is classically described in the literature for suspensions at high crystal concentrations (e.g. [28, 59]). In this study, neither weakening nor hardening have been evidenced, not even in large strain experiments (PO519 – PO524 – PO 528), and duplicate measurements within the same experiment have not shown significant differences in strength (e.g. steps 1 and 4 in PO610 or steps 5 and 7 in PO609).

However, we can conclude that a departure from Newtonian behaviour occurs between $\Phi_s = 0.16$ and 0.34, and that crystal-bearing magmas behave as pseudoplastic materials (possibly viscoplastic) at higher crystal contents, i.e. with a non-linear dependence of shear rate on shear stress (stress exponent > 1). This change in the rheological behaviour between 16 and 34 vol.% of crystals is in good agreement with previous experimental studies [19, 21, 33, 60]. Moreover, if a yield strength exists, it will likely appear in the crystal range ($0.22 \leq \Phi_s \leq 0.29$) predicted by numerical simulations for suspensions containing particles with an aspect ratio of 1 [43, 45].

4.2. Testing Models.

Different models and equations exist for the prediction of the rheology of crystal-bearing magmas [34-40, 61]. Some of these models (e.g. Einstein-Roscoe [34-37] or Costa [61]) are inappropriate for reproducing our data because the dependence of apparent viscosity on shear rate is not taken into account. Moreover, it is widely assumed that the Einstein-Roscoe equation should not be used at crystal concentrations higher than 25 vol.% and Costa's model is not an "absolute" model because several parameters have to be determined by fitting of the data.

We have compared our experimental data with viscosities of magmatic suspensions predicted by the model proposed by Gay et al. [40]. In this model, the yield strength τ_y is given by:

$$\tau_y = 1.26\rho g\left(\frac{D_P}{\Phi_{\max}-\Phi}\right)\left(\frac{\Phi_{\max}}{1-\Phi_{\max}}\right)^2\frac{1}{\xi^{1.5}\sigma^2}, \qquad \text{(E14)}$$

where D_p is the mean diameter of particles and ρ is the density of the fluid. The shape factor (ξ) is defined as the ratio of the surface area of a sphere of equivalent volume to the surface area of the particle. The geometric standard deviation (σ) is estimated from a plot of particle diameters versus cumulative proportion (p) of particles less than a given size. The geometric standard deviation can then be calculated after [62] from:

$$\sigma = (p < 50\%\,\text{size})/(p < 15.87\%\,\text{size})$$

The shear stresses (τ_w) at corresponding strain rates ($\dot{\varepsilon}$) are given by:

$$\tau_w = \dot{\varepsilon}\eta_{\inf} + \frac{(\eta_0-\eta_{\inf})\dot{\varepsilon}}{1+\dot{\varepsilon}(\eta_0-\eta_{\inf})/B} + \tau_y, \qquad \text{(E15)}$$

where η_0 and η_{inf} are the viscosities at low and high strain rate, respectively (see Figure 1 in [33] for the significance of these terms). η_0 and η_{inf} can be calculated from:

$$\eta_0 = \eta_l\left(\frac{\Phi_{\max}}{\Phi_{\max}-\Phi}\right)^{2.5}, \qquad \text{(E16)}$$

$$\eta_{\inf} = \eta_l \exp\left[\left(2.5+\left(\frac{\Phi}{\Phi_{\max}-\Phi}\right)^{0.48}\right)\frac{\Phi}{\Phi_{\max}}\right], \qquad \text{(E17)}$$

where η_l is the viscosity of the liquid phase. B can be calculated from:

$$B = 0.066\left(\frac{\Phi_{\max}^2}{\Phi_{\max}-\Phi}\right)\left(\frac{\eta_l^2}{D_p^2\rho\tau_y}\right)^{0.21}\tau_y, \qquad \text{(E18)}$$

To predict the apparent viscosities corresponding to the experimental conditions in our experiments, the different geometric parameters of the particles were obtained by X-ray microtomography on sample PO514. The High resolution X-ray computed tomography (HRXCT) measurements were performed at the Materials Science Beamline MS of the Swiss Ligth Source (SLS) of the Paul Scherrer Institut (Switzerland). The measurements were conducted on a cylindrical sample, 720 μm in diameter and 10 mm in length [63]. The mean particle diameter D_p is determined to be 48 μm and values of 0.72 and 3.93 are obtained on a population of 339 particles for the shape factor ξ and the geometric standard deviation σ, respectively. The density of the fluid (ρ) is estimated using [64] and the viscosity of the liquid phase (η_l) is obtained using (E11). A plot of measured versus predicted viscosities is shown in Figure 9. Correlation between estimated and measured apparent viscosities is excellent and the equations proposed by [40] reproduce our data within ± 0.5 Log units.

4.3 Maximum Packing Fraction (Φ_m)

The value of Φ_m depends on size, shape and distribution of crystals [21, 38, 39]. In the literature, values of Φ_m range from 0.4 to 0.74, with a classical value of 0.6 for geological materials [41]. In this study, the best fit to our data (E13) gives 0.66 for Φ_m and the best fit with the equations proposed by [40] was obtained with $\Phi_m = 0.74$. These values are sensibly higher than the classical 0.6.

4.4. Correlation between rheological behaviour and development of fabrics.

Shape Preferred Orientations (SPO) of crystals in the samples deformed in this study have been carefully investigated by [48]. A brief summary of the results from that paper is given in this section (see also Figure 14 in [48]). At low crystal content ($\Phi_s = 0.16$), the suspension can be considered as a Newtonian material and a weak and unimodal SPO develops with strain.

Crystal rotation dominates and stream lines of liquid are moderately perturbed by the presence of rigid particles. Some tilling of crystals leads to the formation of small clusters. At $\Phi_s = 0.34$, the rheology departs from Newtonian behaviour (stress exponent $n > 1$). Bimodal SPO develop and trains of colliding particles are observed. At higher crystal content ($\Phi_s = 0.54$ and 0.65), crystal contact interaction dominates and leads to pseudoplastic behaviour of the material (possibly viscoplastic), while the SPO are strongly bimodal and shear bands and S/C like structures develop. No melt segregation in shear bands was identified. Moreover, in the studied material, the SPO remain low even at large strain and seems to have a limited effect on the apparent viscosity of the suspensions.

5 – Conclusion.

In this study, viscosity measurements on magmatic suspensions containing up to 76 vol.% of crystals were performed at 300 MPa confining pressure in the temperature range 450°C-600°C. Effect of crystal concentration and shear stress on the rheological behaviour of magmas was explored, and these two parameters were included as variables in a modified power law fitting our data. Moreover, the observed rheological behaviour is correlated with the development of crystal fabrics (detailed study of Shape Preferred Orientations of crystals presented in a companion paper by [48]). At low crystal concentration ($\Phi_s \leq 0.16$), our magmatic suspensions behave as a Newtonian fluid while a weak and unimodal SPO develops. At higher crystal content, a bimodal SPO develops and the apparent viscosity decreases with increasing applied stress (shear thinning). The apparent viscosity decreases with increasing applied stress (shear thinning). The onset of yield strength, classically described when increasing crystal content, has not been evidenced in this study due to the high stresses applied for the viscosity measurements. No thixotropic behaviour was observed.

In order to determine the existence of a yield strength, viscosity measurements have to be performed at lower stresses. Moreover, to complete this study, experiments with different shapes, sizes and aspect ratios of crystals are needed.

Acknowledgements.

R.C. and L.A. acknowledge support by the French Ministry of Education and Research (ACI JC3013, "Fabriques Magmatiques" and a Ph.D. grant for the first author). M.B. acknowledges support by the Swiss Nationalfond (Project nº 2000-0666.16) in Zurich and by the European Social Fund in Toulouse. R.C. thanks Michel Pichavant and Bruno Scaillet for their help and support during his Ph.D. Comments by Martin O. Saar and an anonymous reviewer were appreciated.

References

[1] H.R. Shaw, Viscosities of magmatic silicate liquids; an empirical method of prediction, Am. J. Sci. 272 (1972) 870-893.

[2] Y. Bottinga, D.F. Weill, The viscosity of magmatic silicate liquids; a model calculation, Am. J. Sci. 272 (1972) 438-475.

[3] D.R. Neuville, P. Richet, Viscosity and mixing in molten (Ca, Mg) pyroxenes and garnets, Geochim. Cosmochim. Acta 55 (1991) 1011-1019.

[4] D.R. Neuville, P. Courtial, D.B. Dingwell, P. Richet, Thermodynamic and rheological properties of rhyolite and andesite melts, Contrib. Mineral. Petrol. 113 (1993) 572-581.

[5] K.U. Hess, D.B. Dingwell, S.L. Webb, The influence of excess alkalis on the viscosity of a haplogranitic melt, Am. Mineral. 80 (1995) 297-304.

[6] D.B. Dingwell, C. Romano, K.U. Hess, The effect of water on the viscosity of a haplogranitic melt under P-T-X conditions relevant to silicic volcanism, Contrib. Mineral. Petrol. 124 (1996) 19-28.

[7] K.U. Hess, D.B. Dingwell, Viscosities of hydrous leucogranitic melts; a non-Arrhenian model, Am. Mineral. 81 (1996) 1297-1300.

[8] D.B. Dingwell, K.U. Hess, Melt viscosities in the system Na-Fe-Si-O-F-Cl; contrasting effects of F and Cl in alkaline melts, Am. Mineral. 83 (1998) 1016-1021.

[9] D.B. Dingwell, K.U. Hess, C. Romano, Viscosities of granitic (sensu lato) melts: Influence of the anorthite component, Am. Mineral. 85 (2000) 1342-1348.

[10] B. Scaillet, A. Whittington, C. Martel, M. Pichavant, F. Holtz, Phase equilibrium constraints on the viscosity of silicic magmas, II: Implications for mafic-silicic mixing processes, Trans.R. Soc. Edinb. 91, Parts 1-2 (2000) 61-72.

[11] A. Whittington, P. Richet, F. Holtz, Water and the viscosity of depolymerized aluminosilicate melts, Geochim. Cosmochim. Acta 64 (2000) 3725-3736.

[12] K.U. Hess, D.B. Dingwell, C. Gennaro, V. Mincione, Viscosity-temperature behaviour of dry melts in the Qz-Ab-Or system, Chem. Geol. 174 (2001) 133-142.

[13] A. Whittington, P. Richet, Y. Linard, F. Holtz, The viscosity of hydrous phonolites and trachytes, Chem. Geol. 174 (2001) 209-223.

[14] D. Giordano, D.B. Dingwell, Non-Arrhenian multicomponent melt viscosity; a model, Earth Planet. Sci. Lett. 208 (2003) 337-349.

[15] M.J. Toplis, D.B. Dingwell, Shear viscosities of CaO-Al_2O_3-SiO_2 and MgO-Al_2O_3-SiO_2 liquids; implications for the structural role of aluminium and the degree of polymerisation of synthetic and natural aluminosilicate melts, Geochim. Cosmochim. Acta 68 (2004) 5169-5188.

[16] G. Sabatier, Recherches sur la déformation sous charge à haute température de quelques roches éruptives, Soc. Franc. Miner., B. 82 (1959) 3-11.

[17] H.R. Shaw, Rheology of basalt in the melting range, J. Petrol. 10 (1969) 510-535.

[18] T. Murase, A.R. McBirney, Properties of Some Common Igneous Rocks and Their Melts at High Temperatures, GSA Bull. 84 (1973) 3563-3592.

[19] F.J. Ryerson, H.C. Weed, A.J. Piwinskii, Rheology of subliquidus magmas, I: Picritic compositions, J. Geophys. Res. 93 (1988) 3421-3436.

[20] N.S. Bagdassarov, D.B. Dingwell, S.L. Webb, Viscoelasticity of crystal- and bubble-bearing rhyolite melts, Phys. Earth Planet. Int. 83 (1994) 83-99.

[21] A.-M. Lejeune, P. Richet, Rheology of crystal-bearing silicate melts; an experimental study at high viscosities, J. Geophys. Res. 100 (1995) 4215-4229.

[22] H. Pinkerton, G. Norton, Rheological properties of basaltic lavas at sub-liquidus temperatures: laboratory and field measurements on lavas from Mount Etna, J. Volcanol. Geotherm. Res. 68 (1995) 307-323.

[23] J. Deubener, R. Bruckner, Influence of nucleation and crystallisation on the rheological properties of lithium disilicate melt, J. Non-Cryst. Solids 209 (1997) 96-111.

[24] T. Lemke, F. Bagusat, K. Kohnke, K. Husemann, H.J. Mogel, Time dependent viscosity of concentrated alumina suspensions, Colloid. Surface. A 150 (1999) 283-287.

[25] Y. Yue, C. Moisescu, G. Carl, C. Rüssel, Influence of suspended iso- and anisometric crystals on the flow behaviour of fluoroapatite glass melts during extrusion, Phys. Chem. Glass. 40 (1999) 243-247.

[26] K. Muller, N.S. Bagdassarov, M. James, H. Schmeling, J. Deubener, Internal friction spectroscopy in Li_2O-$2SiO_2$ partially crystallised glasses, J. Non-Cryst. Solids 319 (2003) 44-56.

[27] H. Sato, Viscosity measurement of subliquidus magmas; 1707 basalt of Fuji Volcano, J. Mineral. Petrol. Sci. 100 (2005) 133-142.

[28] I. Sonder, B. Zimanowski, R. Buettner, Non-Newtonian viscosity of basaltic magma, Geophys. Res. Lett. 33 (2006).

[29] H. Ishibashi, H. Sato, Viscosity measurements of subliquidus magmas: Alkali olivine basalt from the Higashi-Matsuura district, Southwest Japan, J. Volcanol. Geotherm. Res. 160 (2007) 223-238.

[30] J. Renner, B. Evans, G. Hirth, On the rheologically critical melt fraction, Earth Planet. Sci. Lett. 181 (2000) 585-594.

[31] J.P. Burg, J.L. Vigneresse, Non-linear feedback loops in the rheology of cooling-crystallizing felsic magma and heating-melting felsic rock, Deformation Mechanisms, Rheology and Tectonics: Current Status and Future Perspectives, Special Publications 200, Geological Society, London, 2002, pp. 275-292.

[32] C.L. Rosenberg, M.R. Handy, Experimental deformation of partially melted granite revisited; implications for the continental crust, J. Metam. Geol. 23 (2005) 19-28.

[33] H. Pinkerton, R.J. Stevenson, Methods of determining the rheological properties of magmas at sub-liquidus temperatures, J. Volcanol. Geotherm. Res. 53 (1992) 47-66.

[34] A. Einstein, Eine neue bestimmung der molekül-dimensionen, Ann. Phys. 19 (1906) 289-306.

[35] A. Einstein, Berichtigung zu meiner Arbeit: Eine neue Bestimmung der Moleküldimensionen, Ann. Phys. 34 (1911) 591-592.

[36] R. Roscoe, The viscosity of suspensions of rigid spheres, Br. J. Appl. Phys. 3 (1952) 267-269.

[37] R. Roscoe, Suspensions, Flow Properties of Disperse Systems, North-Holland, New-York, 1953.

[38] J.S. Chong, E.B. Christiansen, A.D. Baer, Rheology of concentrated suspensions, J. Appl. Polymer Sci. 15 (1971) 2007-2021.

[39] D.J. Jefferey, A. Acrivos, The rheological properties of suspensions of rigid particles, AIChE J. 22 (1976) 417-432.

[40] E.C. Gay, P.A. Nelson, W.P. Armstrong, Flow properties of suspensions with high solids concentration, AIChE J. 15 (1969) 815-822.

[41] B.D. Marsh, On the crystallinity, probability of occurrence, and rheology of lava and magma, Contrib. Mineral. Petrol. 78 (1981) 85-98.

[42] G.E. Pike, C.H. Seager, Percolation and conductivity: A computer study, Phys. Rev. B 10 (1974) 1421-1433.

[43] E.J. Garboczi, K.A. Snyder, J.F. Douglas, M.F. Thorpe, Geometrical percolation threshold of overlapping ellipsoids, Phys. Rev. E 52 (1995) 819 LP - 828.

[44] C.D. Lorenz, R.M. Ziff, Precise determination of the critical percolation threshold for the three-dimensional "Swiss cheese" model using a growth algorithm, J. Chem. Phys. 114 (2001) 3659-3661.

[45] M.O. Saar, M. Manga, K.V. Cashman, S. Fremouw, Numerical models of the onset of yield strength in crystal-melt suspensions, Earth Planet. Sci. Lett. 187 (2001) 367-379.

[46] M.O. Saar, M. Manga, Continuum percolation for randomly oriented soft-core prisms, Phys. Rev. E 6505 (2002) 6131-6131.

[47] I.M. Krieger, Rheology of monodispersed latices, Adv. Colloid Interfac. Sci. 3 (1972) 111-136.

[48] L. Arbaret, M. Bystricky, R. Champallier, Microstructures and rheology of hydrous synthetic magmatic suspensions deformed in torsion at high pressure., J. Geophys. Res. 112 (2007) B10208.

[49] C. Martel, D.B. Dingwell, O. Spieler, M. Pichavant, M. Wilke, Experimental fragmentation of crystal- and vesicle-bearing silicic melts, Bull. Volcanol. 63 (2001) 398-405.

[50] F. Holtz, W. Johannes, M. Pichavant, Effect of excess aluminium on phase relations in the system Qz-Ab-Or – Experimental investigation at 2 kbar and reduced H_2O activity, Eur. J. Mineral. 4 (1992) 137-152.

[51] H. Behrens, Determination of water solubilities in high-viscosity melts; an experimental study on $NaAlSi_3O_8$ and $KAlSi_3O_8$ melts, Eur. J. Mineral. 7 (1995) 905-920.

[52] H. Behrens, M. Nowak, Quantification of H_2O speciation in silicate glasses and melts by IR spectroscopy - In situ versus quench techniques, Phase Transit. 76 (2003) 45-61.

[53] P. Richet, A. Whittington, F. Holtz, H. Behrens, S. Ohlhorst, M. Wilke, Water and the density of silicate glasses, Contrib. Mineral. Petrol. 138 (2000) 337-347.

[54] M.S. Paterson, D.L. Olgaard, Rock deformation tests to large shear strains in torsion, J. Struct. Geol. 22 (2000) 1341-1358.

[55] H.J. Frost, M.F. Ashby, Deformation-mechanism maps: The plasticity and creep of metals and ceramics, Pergamon Press, New York, 1982, 167 pp.

[56] J.E. Dorn, Some fundamental experiments on high-temperature creep. Creep and fracture of metals at high tempertures, in: NPL symposium, HMSO, London, 1956, pp. 89-138.

[57] T. Dabak, O. Yucel, Modeling of the concentration particle size distribution effects on the rheology of highly concentrated suspensions, Powder Technol. 52 (1987) 193-206.

[58] C.K. Kerr, J.R. Lister, The effects of shape on crystal settling and on the rheology of magmas, J. Geol. 99 (1991) 457-467.

[59] N. Bagdassarov, H. Pinkerton, Transient phenomena in vesicular lava flows based on laboratory experiments with analogue materials, J. Volcanol. Geotherm. Res. 132 (2004) 115-136.

[60] D.B. Marsh, Magmatic processes, Rev. geophys. 25 (1987) 1043-1053.

[61] A. Costa, Viscosity of high crystal content melts: Dependence on solid fraction, Geophys. Res. Lett. 32 (2005) L22308.

[62] J.E. Smith, M.L. Jordan, Mathematical and graphical interpretation of the log normal law for particle size distribution analysis, J. Colloid Sci. 19 (1964) 549-559.

[63] L. Arbaret, Three-dimensional grain fabric and clustering analysis by synchrotron-based X-ray tomography in a magmatic suspensions deformed in torsion at high pressure, in preparation for Geophys. Res. Lett. (2007).

[64] R. Knoche, D.B. Dingwell, S.L. Webb, Melt densities for leucogranites and granitic pegmatites: Partial molar volumes for SiO_2, Al_2O_3, Na_2O, K_2O, Li_2O, Rb_2O, Cs_2O, MgO, CaO, SrO, BaO, B_2O_3, P_2O_5, $F2O_{-1}$, TiO_2, Nb_2O_5, Ta_2O_5, and WO_3, Geochim. Cosmochim. Acta 59 (1995) 4645-4652.

Figure captions

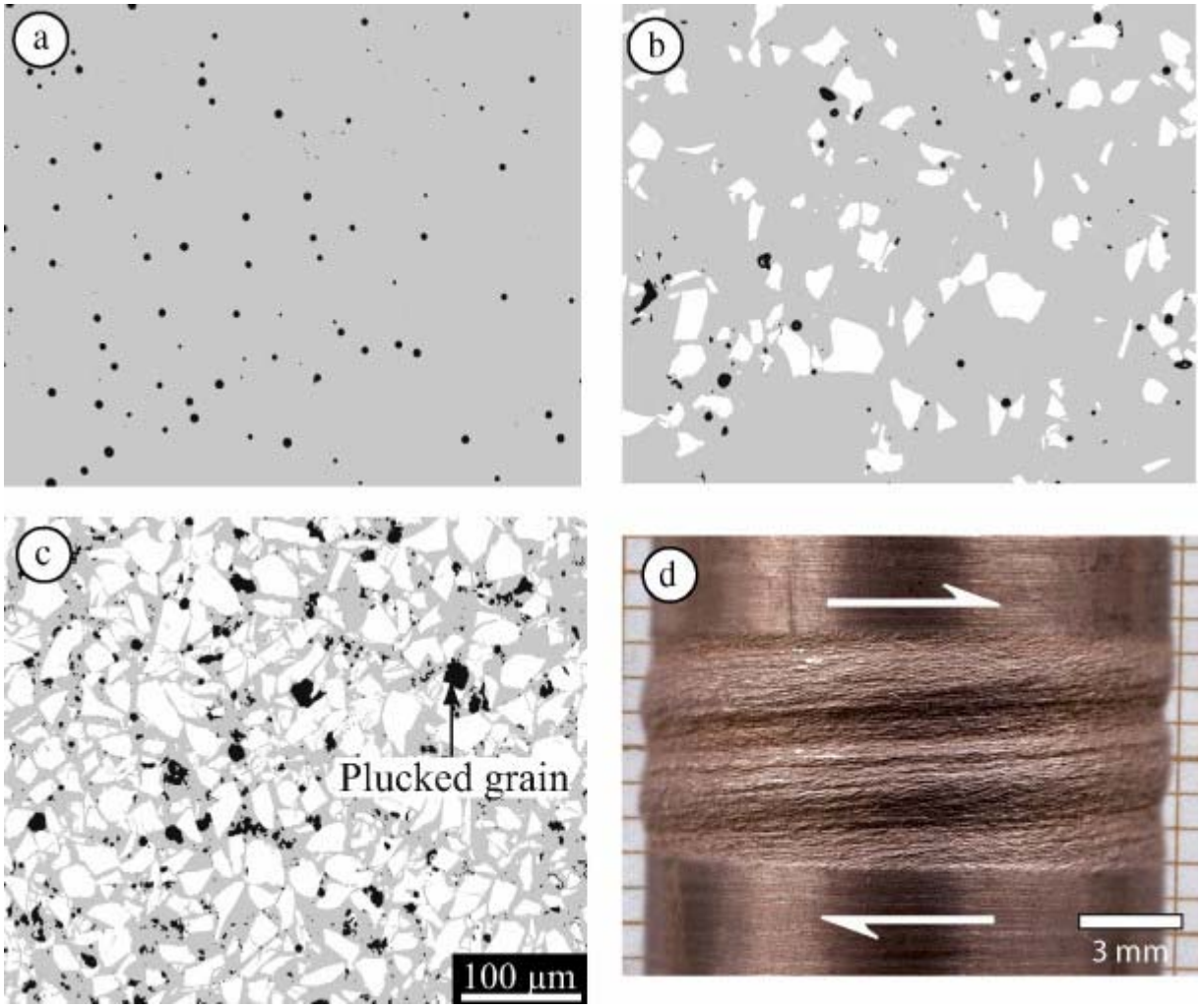

Figure 1: (a-c) Scanning Electron Microprobe images of starting products: Samples HPG10, HPG5 and HPG8 containing 0, 16 and 54 vol. % of crystals, respectively (Photo a, b and c, respectively). White = Crystals, Grey = Melt, Black = bubbles (and plucked crystals in sample HPG8). Scale is common to the 3 images. (d) Sample in its jacket after deformation experiment (PO519).

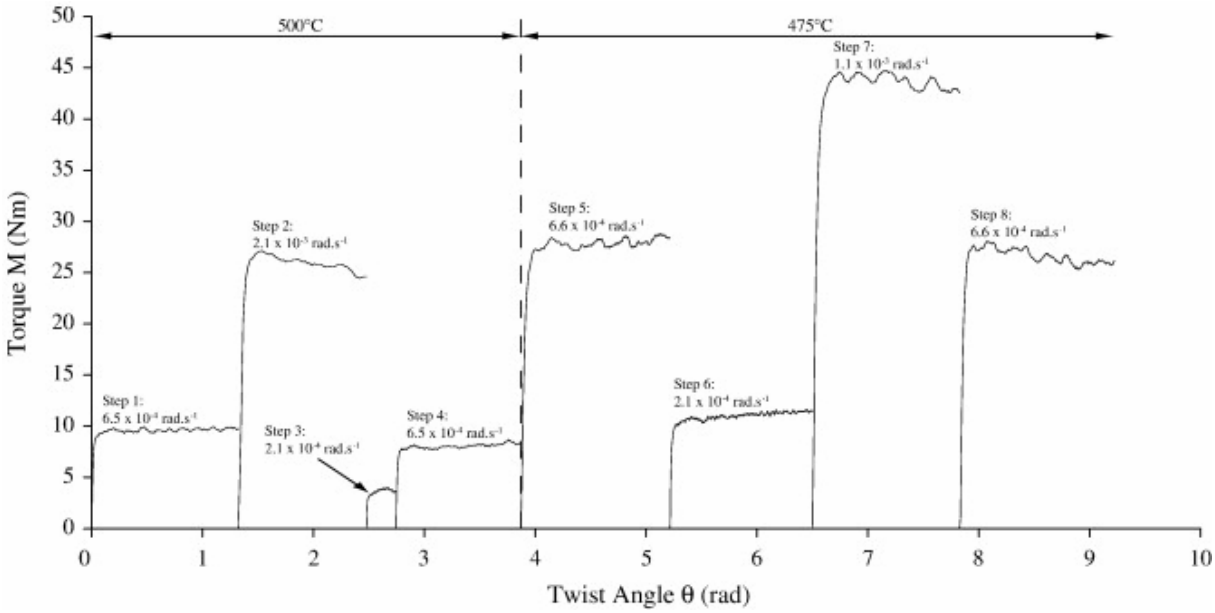

Figure 2: Torque m (Nm) versus twist angle θ (rad) for a multi-step experiment (PO540). Steps 1 to 4 were run at 500°C and steps 5 to 8 at 475°C.

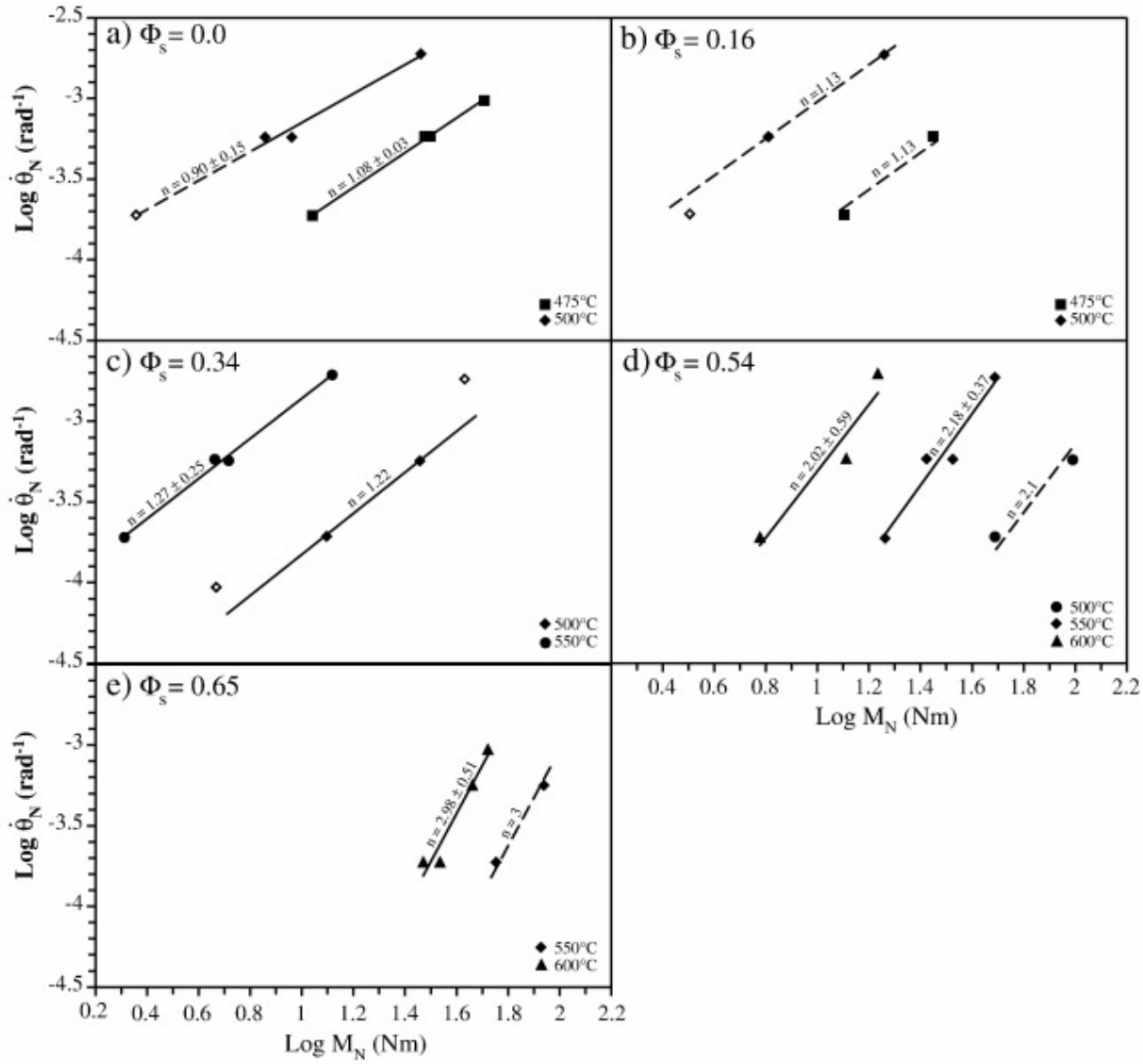

Figure 3: Log-Log plot of normalized twist rate $\dot{\theta}_N$ (rad^{-1}) versus normalized torque M_N (Nm) for hydrated crystal free melt ($\Phi_s = 0$) and crystal-bearing magmas with crystal contents up to 65 vol.% ($\Phi_s = 0.16$ - 0.65). Twist rate and torque were normalized to a sample of 15 mm in diameter and 7 mm in length following (E5) and (E6). For each temperature and composition, the slope of the line corresponds to the stress exponent *n*. Open symbols indicate values not used for the calculations and dashed lines are extrapolated from data at other twist rate or temperature conditions (see text for further details).

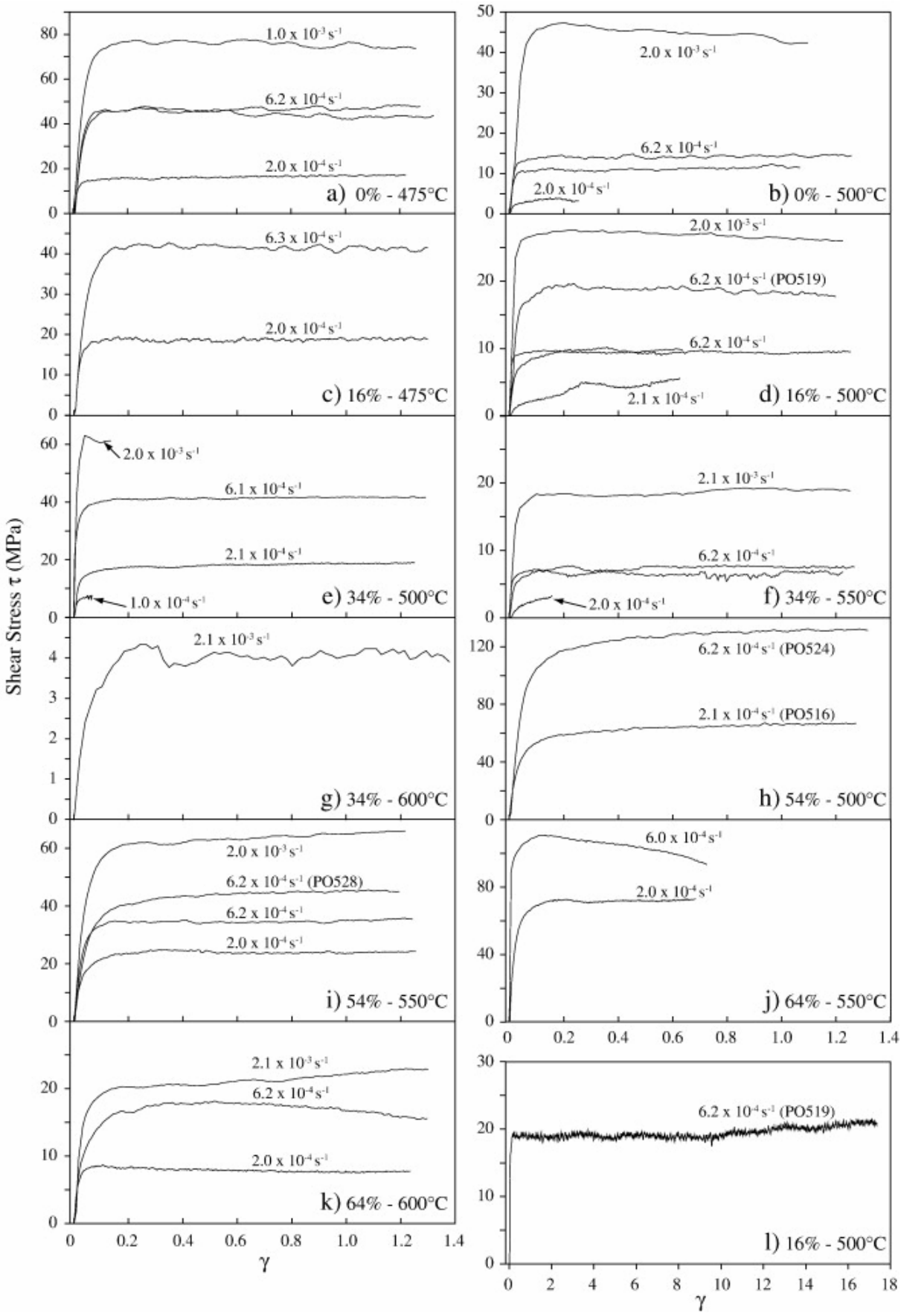
Shear Stress τ (MPa)
γ
a) 0% - 475°C
1.0 x 10⁻³ s⁻¹
6.2 x 10⁻⁴ s⁻¹
2.0 x 10⁻⁴ s⁻¹
b) 0% - 500°C
2.0 x 10⁻³ s⁻¹
6.2 x 10⁻⁴ s⁻¹
2.0 x 10⁻⁴ s⁻¹
c) 16% - 475°C
6.3 x 10⁻⁴ s⁻¹
2.0 x 10⁻⁴ s⁻¹
d) 16% - 500°C
2.0 x 10⁻³ s⁻¹
6.2 x 10⁻⁴ s⁻¹ (PO519)
6.2 x 10⁻⁴ s⁻¹
2.1 x 10⁻⁴ s⁻¹
e) 34% - 500°C
2.0 x 10⁻³ s⁻¹
6.1 x 10⁻⁴ s⁻¹
2.1 x 10⁻⁴ s⁻¹
1.0 x 10⁻⁴ s⁻¹
f) 34% - 550°C
2.1 x 10⁻³ s⁻¹
6.2 x 10⁻⁴ s⁻¹
2.0 x 10⁻⁴ s⁻¹
g) 34% - 600°C
2.1 x 10⁻³ s⁻¹
h) 54% - 500°C
6.2 x 10⁻⁴ s⁻¹ (PO524)
2.1 x 10⁻⁴ s⁻¹ (PO516)
i) 54% - 550°C
2.0 x 10⁻³ s⁻¹
6.2 x 10⁻⁴ s⁻¹ (PO528)
6.2 x 10⁻⁴ s⁻¹
2.0 x 10⁻⁴ s⁻¹
j) 64% - 550°C
6.0 x 10⁻⁴ s⁻¹
2.0 x 10⁻⁴ s⁻¹
k) 64% - 600°C
2.1 x 10⁻³ s⁻¹
6.2 x 10⁻⁴ s⁻¹
2.0 x 10⁻⁴ s⁻¹
l) 16% - 500°C
6.2 x 10⁻⁴ s⁻¹ (PO519)

Figure 4: Shear stress τ (MPa) versus shear strain γ curves obtained between 475°C and 600°C for hydrated crystal free melt (Φ_s = 0) and crystal-bearing magmas with crystal contents up to 65 vol.% (Φ_s = 0.16 - 0.65).

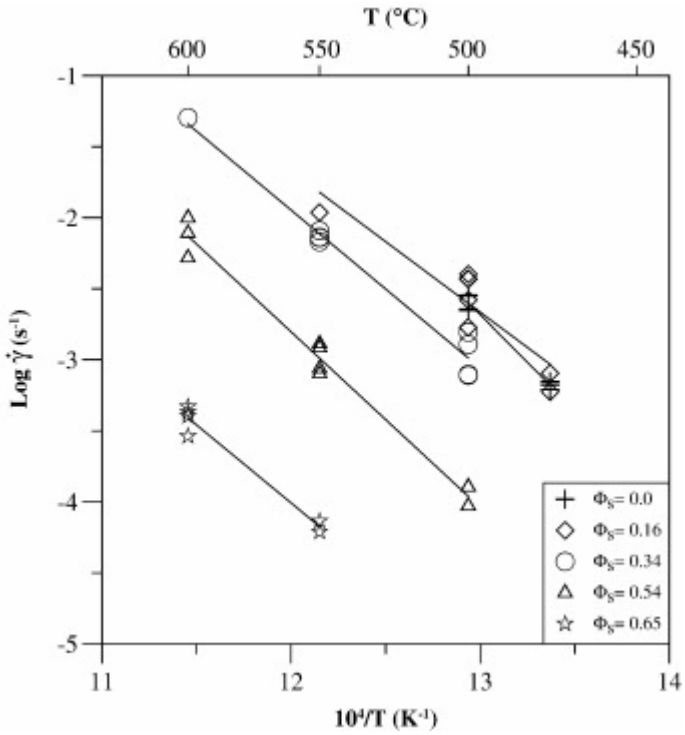

Figure 5: Shear rate as a function of reciprocal temperature. Data were normalized to 50 MPa using the stress exponents *n* presented in table 3. The activation energies *Q* are calculated from this diagram and (E9).

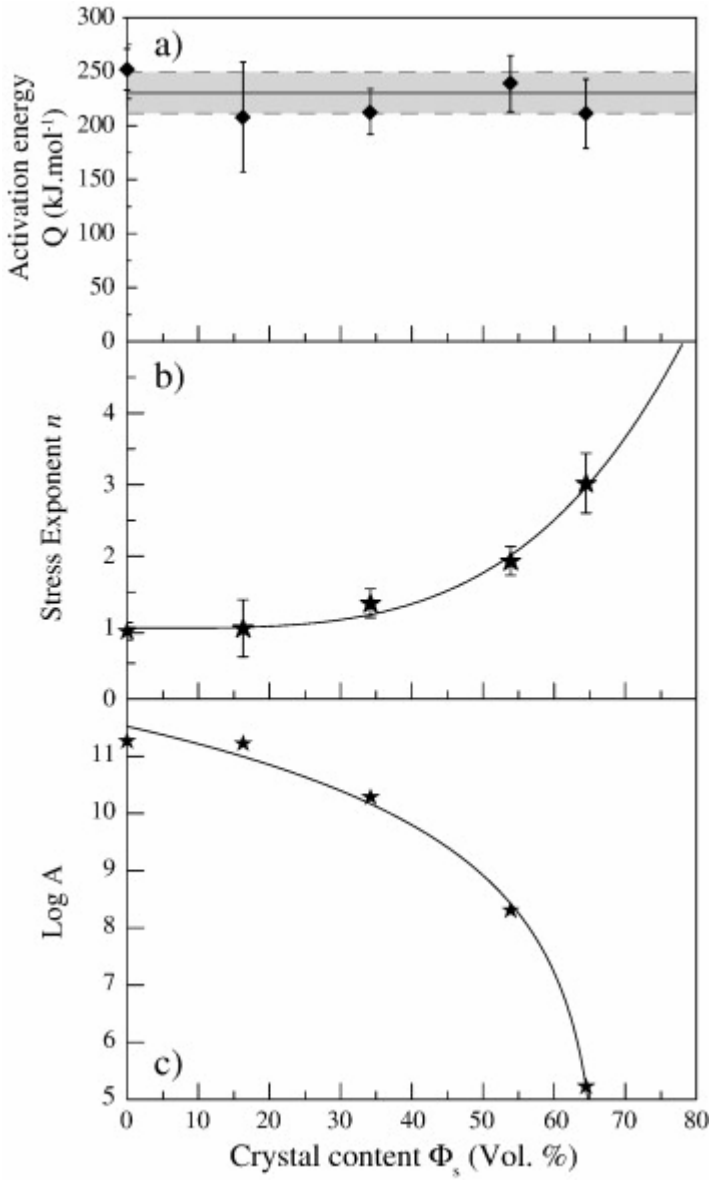

Figure 6: Activation energy Q (a), stress exponent n (b) and preexponential term A (c) as a function of crystal content. The solid lines represent the fits obtained using (E12) and (E13) with $Q = 231 \pm 19$ kJ.mol^{-1}.

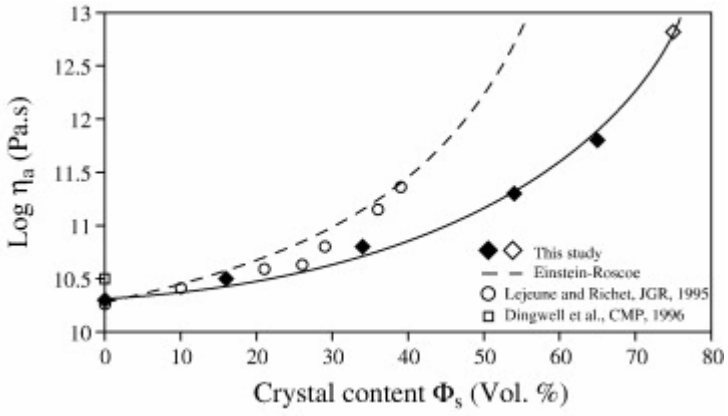

Figure 7: Apparent viscosity η_a (Pa.s) versus crystal content Φ_s(vol.%) at 500°C and a shear rate of 6 x 10^{-4} s^{-1} (diamonds; filled diamonds: measured; open diamonds: estimated from E11 and table 3; solid line: E11). The viscosity for a pure ($\Phi s = 0$) haplogranitic melt with 2.3 wt. % of water at 502°C measured by [6] (open square) and viscosities for partially crystallised $Mg_3Al_2Si_3O_{12}$ melts at 800°C measured by [21] (open circles) are also reported. The Einstein-Roscoe model with classical values for k and Φ_m (2.5 and 0.6, respectively) is given in dashed line.

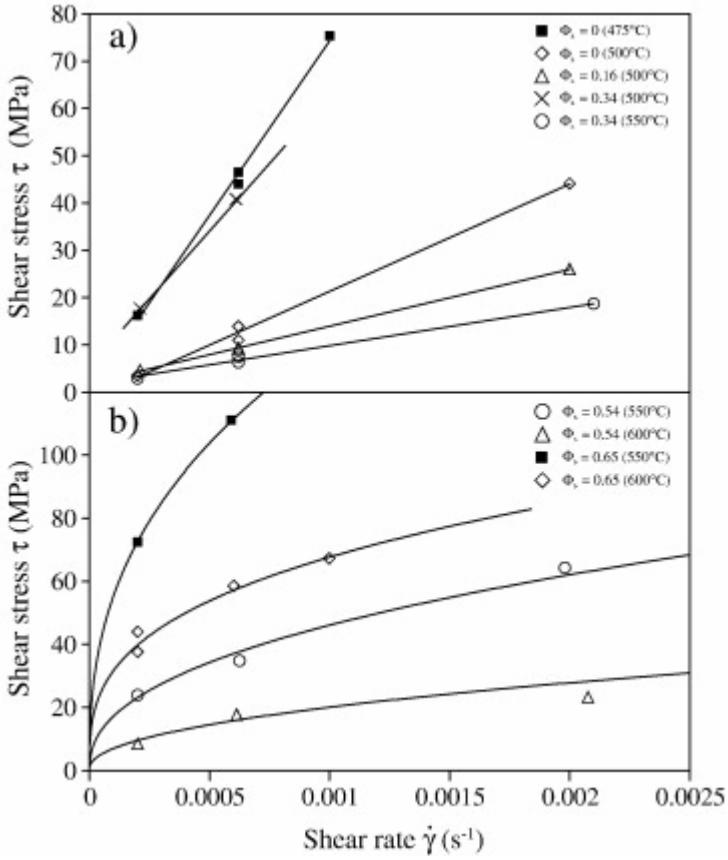

Figure 8: Shear stress versus Shear rate at low (a) and high (b) crystal content. Data reported for Fs = 0.16 and 500°C are those obtained in run PO610 with a sample containing 3 wt. % of water instead of 2.5 wt. % for other experiments. At high crystal fraction, data were fitted using a power-law model (E11 and table 3). Data at lower stresses are required to determine if a yield-power law would be more appropriate.

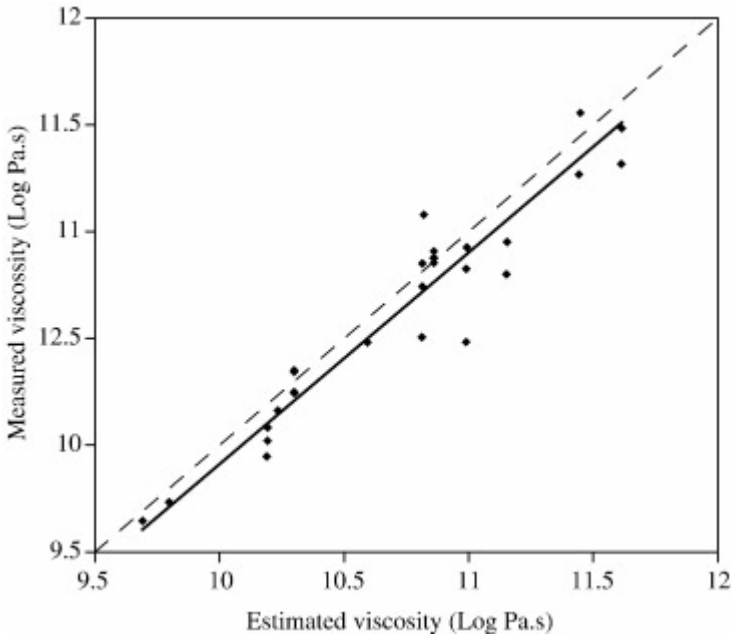

Figure 9: Plot of viscosities measured in this study (values from table 2) versus viscosities estimated at our experimental conditions using [40].

Table 1: Characteristics of starting samples and experimental conditions for viscosity measurements.

Run	Φ_S (Vol. %)	Starting Sample	H_2O (wt%) KFT[(1)(2)]	H_2O (wt%) IR[(1)(3)]	Length (mm)	Diameter (mm)	Jacket	P (MPa)	T (°C)	Strain rate (s^{-1})	Finite strain (γ)
PO540	0	HPG - 10a	2.57	2.45	7.84	14.87	Cu	300	475-500	$2x10^{-4}$ - $2x10^{-3}$	8.8
PO514	16.3	HPG - 5a	2.60	2.47	7.064	14.91	Cu	300	475	$2x10^{-4}$ - $6x10^{-4}$	2.6
PO519	16.3	HPG - 5b	2.60	2.65	6.635	14.94	Cu	300	500-550	$6x10^{-4}$	17.5
PO610	16.3	HPG - 11a	*3.0*	*2.84*	8.495	14.92	Cu	300	500-550	$2x10^{-4}$ - $2x10^{-3}$	7.0
PO609	34.2	HPG - 8	nd	nd	9.662	14.93	Cu	300	500-600	$1x10^{-4}$ - $2x10^{-3}$	8.5
PO516	53.9	HPG - 6a	2.61	nd	9.794	14.91	Cu	300	500-600	$2x10^{-4}$ - $2x10^{-3}$	10.8
PO524	53.9	HPG - 6b	2.55	nd	5.592	11.80	Cu	300	500	$6x10^{-4}$	8.8
PO528	53.9	HPG - 6c	2.45	nd	5.013	14.90	Cu	300	550	$6x10^{-4}$	21.3
PO612	64.5	HPG - 13	2.47	nd	9.865	7.96	Cu	300	500-600	$2x10^{-4}$ - $1x10^{-3}$	6.5
PO515	75.7	HPG - 7a	2.33	nd	11.531	14.90	Fe	300	800-1000	$2x10^{-5}$ - $2x10^{-4}$	0.05

(1) Determined on starting products. (2) After correction for crystal content. (3) At crystal contents higher than 16 vol. %, crystal-free areas were too small to allow water content determination.

Table 2: Viscosity data.

Run	Φ_s (Vol.%)	T (°C)	Step	$\dot{\theta}$ (rad.s^{-1})	Torque m (N.m)	Jacket Signal (N.m)	Strain rate $\dot{\gamma}$ (s^{-1})	Stress τ (MPa)	Apparent Viscosity η_a (Log Pa.s)	Step strain (γ)
PO540	0	500	1	$6.5x10^{-4}$	8.9 ± 0.2	2.8	$6.2x10^{-4}$	13.9 ± 0.3	10.35 ± 0.01	1.26
			2	$2.1x10^{-3}$	28.2 ± 0.8	3.4	$2.0x10^{-3}$	44.1 ± 1.3	10.31± 0.01	1.09
			3	$2.1x10^{-4}$	2.2 ± 0.1(1)	2.4	$2.0x10^{-4}$	3.5 ± 0.2(1)	10.28 ± 0.03(1)	0.25
			4	$6.5x10^{-4}$	7.0 ± 0.2	2.8	$6.2x10^{-4}$	11.0 ± 0.4	10.28 ± 0.02	1.07
		475	5	$6.6x10^{-4}$	30.7 ± 0.5	3.3	$6.2x10^{-4}$	46.5 ± 0.8	10.87 ± 0.01	1.27
			6	$2.1x10^{-4}$	10.7 ± 0.4	2.7	$2.0x10^{-4}$	16.2 ± 0.6	10.93 ± 0.01	1.22
			7	$1.1x10^{-3}$	49.8 ± 0.8	3.5	$1.0x10^{-3}$	75.3 ± 1.2	10.86 ± 0.03	1.26
			8	$6.6x10^{-4}$	29.2 ± 0.9	3.3	$6.2x10^{-4}$	44.2 ± 1.3	10.83 ± 0.02	1.32
PO514	0.16	475	1	$5.9x10^{-4}$	27.9 ± 0.3	4.1	$6.3x10^{-4}$	39.8 ± 0.5	10.80 ± 0.01	1.27
			2	$1.9x10^{-4}$	12.6 ± 0.2	3.4	$2.0x10^{-4}$	17.9 ± 0.3	10.94 ± 0.01	1.27
PO519	0.16	550	1	$5.4x10^{-4}$	2.3 ± 0.1(1)	2.8	$6.1x10^{-4}$	3.3 ± 0.2(1)	9.73 ± 0.03(1)	0.30
		500	2	$5.5x10^{-4}$	13.1 ± 1.2	3.6	$6.2x10^{-4}$	18.8 ± 1.8	10.50 ± 0.04	17.19
PO610	0.16	500	1	$7.1x10^{-4}$	6.4 ± 0.2	3.5	$6.2x10^{-4}$	9.2 ± 0.2	10.17 ± 0.01	1.25
			2	$2.3x10^{-3}$	18.0 ± 0.3	4.2	$2.0x10^{-3}$	26.0 ± 0.5	10.11 ± 0.01	1.22
			3	$2.3x10^{-4}$	3.2 ± 0.3	3.0	$2.1x10^{-4}$	4.6 ± 0.4	10.35 ± 0.04	0.63
			4	$7.1x10^{-4}$	6.4 ± 0.1	3.5	$6.2x10^{-4}$	9.3 ± 0.2	10.17 ± 0.01	0.63
		550	5	$7.2x10^{-4}$	1.5(1)	2.8	$6.3x10^{-4}$	2.2(1)	9.5(1)	0.34
			6	$1.1x10^{-3}$	2.8(1)	3.0	$1.0x10^{-3}$	4.0(1)	9.6(1)	0.64
			7	$2.3x10^{-3}$	nd(1)	3.3	$2.1x10^{-3}$	nd(1)	nd(1)	2.31
PO609	0.34	500	1	$2.7x10^{-4}$	12.3 ± 0.5	3.0	$2.1x10^{-4}$	17.7 ± 0.7	10.93 ± 0.02	1.25
			2	$7.9x10^{-4}$	28.3 ± 0.2	3.6	$6.1x10^{-4}$	40.8 ± 0.3	10.82 ± 0.01	1.29
			3	$2.5x10^{-3}$	42.2 ± 1.1(2)	4.3	$2.0x10^{-3}$	60.8 ±1.6(2)	10.49 ± 0.01(2)	0.01
		550	4	$2.6x10^{-4}$	2.0 ± 0.1(1)	2.4	$2.0x10^{-4}$	2.9 ± 0.1(1)	10.15 ± 0.02(1)	0.16
			5	$8.0x10^{-4}$	4.5 ± 0.2	2.8	$6.2x10^{-4}$	6.5 ± 0.3	10.02 ± 0.02	1.28
			6	$2.7x10^{-3}$	12.9 ± 0.3	3.4	$2.1x10^{-3}$	18.6 ± 0.4	9.95 ± 0.01	1.30
			7	$8.0x10^{-4}$	5.2 ± 0.2	2.8	$6.2x10^{-4}$	7.5 ± 0.2	10.08 ± 0.01	1.32
		600	8	$2.7x10^{-3}$	2.8 ± 0.1	2.7	$2.1x10^{-3}$	4.0 ± 0.1	9.29 ± 0.01	1.80
		500	9	$1.3x10^{-4}$	4.6 ± 0.3(3)	2.7	$1.0x10^{-4}$	6.6 ± 0.4(3)	10.82 ± 0.03(3)	0.07
PO516	0.54	500	1	$2.7x10^{-4}$	48.3 ± 1.8	3.0	$2.1x10^{-4}$	64.1 ± 2.4	11.49 ± 0.02	1.27
		550	2	$2.7x10^{-4}$	18.1 ± 0.4	2.4	$2.0x10^{-4}$	24.0 ± 0.5	11.08 ± 0.01	1.25
			3	$8.2x10^{-4}$	26.2 ± 0.3	2.8	$6.3x10^{-4}$	34.8 ± 0.4	10.74 ± 0.01	1.24
			4	$2.6x10^{-3}$	48.3 ± 1.0	3.4	$2.0x10^{-3}$	64.1 ± 1.36	10.51 ± 0.01	1.21
		600	5	$8.2x10^{-4}$	12.8 ± 0.6	2.3	$6.2x10^{-4}$	17.2 ± 0.8	10.44 ± 0.02	1.28
			6	$2.7x10^{-4}$	5.9 ± 0.2	1.9	$2.0x10^{-4}$	8.0 ± 0.3	10.60 ± 0.01	1.22
			7	$2.7x10^{-3}$	17.0 ± 0.8	2.7	$2.1x10^{-3}$	22.9 ± 1.1	10.04 ± 0.02	3.35
PO524	0.54	500	1	$5.9x10^{-4}$	48.0 ± 1.5	1.9	$6.2x10^{-4}$	128.5 ± 4.1	11.32 ± 0.01	8.76
PO528	0.54	550	1	$4.2x10^{-4}$	33.1 ± 0.9	2.0	$6.2x10^{-4}$	44.0 ± 1.2	10.85 ± 0.01	21.26
PO612	0.65	500	1	$5.0x10^{-4}$	10.3(2)	1.1	$2.0x10^{-4}$	87.3(2)	11.64(2)	nd(2)
			2	$1.5x10^{-3}$	10.7(2)	1.3	$6.0x10^{-4}$	90.6(2)	11.18(2)	nd(2)
		600	3	$5.0x10^{-4}$	5.2	0.7	$2.0x10^{-4}$	43.9	11.34	0.10
			4	$1.5x10^{-3}$	6.9	0.8	$6.0x10^{-4}$	58.6	10.99	1.21
			5	$5.0x10^{-4}$	4.5	0.7	$2.0x10^{-4}$	37.8	11.28	0.70

	6	$2.5x10^{-3}$	8.0	0.9	$1.0x10^{-3}$	67.3	10.83	1.24
550	7	$5.0x10^{-4}$	8.6	0.9	$2.0x10^{-4}$	72.4	11.56	0.65
	8	$1.5x10^{-3}$	13.1	1.0	$6.0x10^{-4}$	111.2	11.27	0.73
	9	$2.5x10^{-3}$	12.9(2)	1.1	$1.0x10^{-3}$	109.2(2)	11.04(2)	nd(2)
500	10	$5.0x10^{-4}$	13.1(2)	1.1	$2.0x10^{-4}$	110.6(2)	11.74(2)	nd(2)
	11	$1.5x10^{-3}$	14.4(2)	1.3	$6.0x10^{-4}$	121.6(2)	11.31(2)	nd(2)
	12	$1.5x10^{-3}$	15.2(2)	1.3	$6.0x10^{-4}$	129.0(2)	11.33(2)	nd(2)

(1) Data were considered to be below the detection range of the apparatus when the jacket signal was higher than 50% of the total measured torque. (2) Data not used for calculations. Slip between alumina pistons occurred during these steps (see text for further details). (3) Step probably too short to allow steady state to be reached (maximum torque probably not registered). Data not used for calculation.

Table 3: Flow law parameters for magmas with different solid fractions Φ_s: activation energy Q, stress exponent n and preexponential term A.

Φ_s (vol.%)	Q ($kJ.mol^{-1}$)(1)	n(2)	Log A ($MPa^{-n}.s^{-1}$)(3)
0	252 ± 19	0.95 ± 0.06	11.27 ± 0.09
16	208 ± 51	0.99 ± 0.20	11.23 ± 0.23
34	213 ± 21	1.34 ± 0.10	10.29 ± 0.12
54	239 ± 26	1.93 ± 0.10	8.31 ± 0.16
65	211 ± 32	3.02 ± 0.21	5.23 ± 0.37

(1) Calculated from Figure 5 and equation (9). (2) Calculated with constant Q = 231 kJ mol^{-1}. Do not correspond to the mean values reported in Figure 3. (3) Calculated with Q = 231 kJ mol^{-1} and stress exponents reported in this table.